



## The effect of cobalt addition on the meso-porous structured $\gamma$ -Alumina synthesized by aqueous sol-gel method

*Manoochehr Sobhani\**, *Hossein Tavakoli*

*Faculty of Materials & Metallurgical Engineering, Semnan University, Semnan, Iran.*

*Received: 02 January 2019; Accepted: 09 April 2019*

*\* Corresponding author email: [m.sobhani@semnan.ac.ir](mailto:m.sobhani@semnan.ac.ir)*

### ABSTRACT

In the present study, the gamma alumina ( $\gamma$ -Al<sub>2</sub>O<sub>3</sub>) nano powders have been prepared with addition of 1%mol Co using an aqueous sol-gel method at lower temperature than the pure gamma alumina. The synthesis process accomplished by partial hydrolysis of the aqueous solution of metallic ions Al<sup>3+</sup> and Co<sup>2+</sup>, with ammonia. The Al(NO<sub>3</sub>)<sub>3</sub>.9H<sub>2</sub>O and Co(NO<sub>3</sub>)<sub>2</sub>.6H<sub>2</sub>O salts were used as cations sources. The obtained gel at 40 °C dried at 120°C and calcined at different temperatures. X-ray diffraction (XRD), scanning electron microscopy (SEM), transmission electron microscopy (TEM) and BET method of surface analysis were applied for powders characterization. The results indicated that the well crystallization of the gamma phase occurred at about 700°C for the Co doped samples while it was 900 °C for the pure sample. The specific surface area and particle sizes of the powders varied from 186 to 140 m<sup>2</sup>/g and 8 to 11 nm for pure and cobalt added  $\gamma$ -Al<sub>2</sub>O<sub>3</sub>, respectively. Both powders have the meso-porous structure according to the hysteresis loop of the adsorption/desorption curves of BET analysis. In addition, the TEM diffraction pattern of the gamma alumina at the presence of Co contains some bright diffracted points due to its higher degree of crystallinity in comparison with the pure powder.

**Keywords:** *Synthesis, Meso-porous, Aqueous Sol-gel,  $\gamma$ -Alumina .*

### 1- Introduction

Alumina (Al<sub>2</sub>O<sub>3</sub>) has different transition phases that converted to another with temperature increasing. Crystalline phases formation accompanied with thermal dehydroxylation of the aluminum hydroxides or oxyhydroxide in a temperature range of about 300-600°C [1, 2]. All of them transformed to  $\alpha$ -alumina at about 1100°C [3-5]. From them,  $\gamma$ -alumina has been shown to be significant industrial catalysts or catalyst substrate in chemical processes [6-8]. It used as a support for cobalt based catalysts in the Fischer-Tropsch (FT) method to production of the clean fuels [9, 10]. The development of the  $\gamma$ -alumina supported

catalysts containing cobalt, molybdenum, iron or copper according to their evaluation in the oxidative desulphurization process of diesel fuel have been widely investigated [11-15]. There are several methods of wet chemistry such as sol-gel, combustion and precipitation based on alumina salts in aqueous or non-aqueous systems for synthesis of gamma alumina phase [6, 16-18]. At the combustion synthesis slow decomposition at low pH values 2, 4 and 6 obtained flaky powders and the rapid decomposition at high pH = 10 cause to make fine powders [16]. Morphological controlling of synthesized alumina powders has attracted the attentions due to its different interesting

properties [8, 19]. The authors achieved to the wormlike  $\gamma$ - $\text{Al}_2\text{O}_3$  with meso-porous channels after calcinations of the prepared precursors from ionic liquid [Bmim]PF<sub>6</sub> and Aluminum isopropoxide at about 600 °C [20]. In another combustion procedure at the presence of the urea and glycine as fuel and  $\text{Al}(\text{NO}_3)_3$  as oxidizer, the pure gamma alumina phase obtained directly at an optimum ratio of the urea to glycine with average crystallite size of about 5 nm [21]. Simultaneous addition of the anionic and non-ionic surfactant to the alumina sol resulted in formation of alumina nano-rods with about 30 m<sup>2</sup>/g of specific surface for calcined powders at 1000 °C [22]. Precipitation of the aluminum nitrate solution with different precipitating agent such as  $\text{NaHCO}_3$ ,  $(\text{NH}_4)_2\text{CO}_3$ ,  $\text{Na}_2\text{CO}_3$  and  $\text{NH}_4\text{HCO}_3$  leads to formation of the boehmite phase and gamma alumina obtained after calcination of the boehmite at 550°C [23]. Therefore, regarding to the literature due to the importance of the metallic ions presence (such as cobalt cations) in the  $\gamma$ - $\text{Al}_2\text{O}_3$  phase, as a novelty in the present study synthesis and characterization of the  $\gamma$ -alumina with addition of cobalt cations have been investigated. Also, synthesis with low-cost raw materials and simple sol-gel method followed up.

## 2- Materials and methods

The starting used raw materials of the present work were aluminum nitrate ( $\text{Al}(\text{NO}_3)_3 \cdot 9\text{H}_2\text{O}$ ,

98.5%) and cobalt nitrate ( $\text{Co}(\text{NO}_3)_2 \cdot 6\text{H}_2\text{O}$ ). Also, ammonia solution 25% was used as basic addition for cation hydrolysis process step. The flowchart of the synthesis procedure is shown in Fig. 1. All of them were purchased from Merck chemical company Germany. At first About 7.5 g (0.02 mol) of aluminum nitrate (0.01 mol of alumina) was dissolved in 50 cc of de-ionized water and 0.029 g (0.0001 mol) of cobalt nitrate was added slowly under continuous magnetic stirring. The solution was maintained for 2 hours under stirring. The molar ratio of the basic agent to Al cations was 1:3, lower than the enough amount of the fully hydrolyzation, according to the below equation [23] :



Hence, diluted ammonia introduced drop-wise to the solution under continues magnetic stirring at 40 °C for 4 h. The obtained concentrated gel was dried at 120 °C. To avoid the risk of the explosive nitrate decomposition, the gel was heated to 250 °C for 2 h. The dried product calcined at 550, 700 and 850 °C in an electrical furnace at air atmosphere to obtain the final powders. The heating rate was 10 °C/min with soaking time of 2 h.

X-ray diffractometer (XRD), (Model: Siemens D-500) with  $\text{CuK}_\alpha$  ( $\lambda=1.54 \text{ \AA}$ ) radiation was applied to phase determination of the powders.

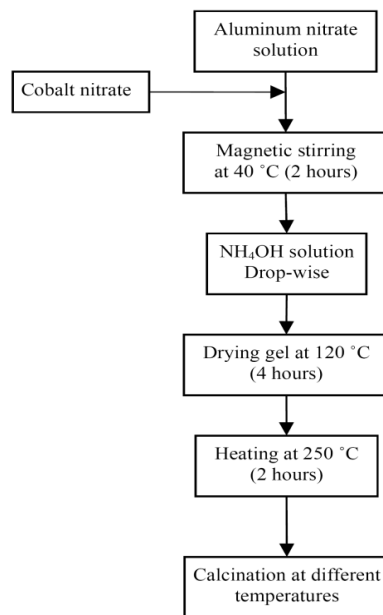


Fig. 1- Flowchart of the aqueous sol-gel process of Co-doped  $\gamma$ -alumina.

Crystallite size of the synthesized powders ( $G_{XRD}$ ) was measured by the Scherrer formula [22]. Additionally, to eschew the instrumental broadening of the diffracted peak, obtained  $B(2\theta)$  was refined using the FWHMs of the standard silicon sample. The Brunauer–Emmett–Teller (BET) method with nitrogen gas adsorption, using a surface area analyzer (Model: BELSORP II) was used for specific surface area (SSA) and pore size distribution determination of the synthesized powders. The size of the particles ( $G_{BET}$ ) was calculated from the BET results regarding to the following equation [24]:

$$G_{BET} = \frac{6}{\rho_{\gamma\text{-Alumina}} \text{SSA}} \quad (\text{eq. 2})$$

Where:  $\rho_{\gamma\text{-Alumina}}$  is the density of the  $\gamma$ -alumina and SSA is the specific surface area ( $\text{m}^2/\text{g}$ ) of the powders. Observational microstructure studies were done by field emission scanning electron microscopy (FESEM) apparatus (Model: MIRA II). Transmission electron microscope (TEM) model: PHILIPS-CM3U was used to structural and size examination of the samples. For the sample preparation first, the powders were ultrasonically dispersed into absolute ethanol and the resultant suspension was spread on the surface of a copper grid. The camera length was 175 mm and acceleration voltage was 150 kV.

### 3- Results and discussions

Figure 2 shows the X-ray diffraction analysis results for sample A, that prepared without cobalt addition and calcined at various temperatures. It

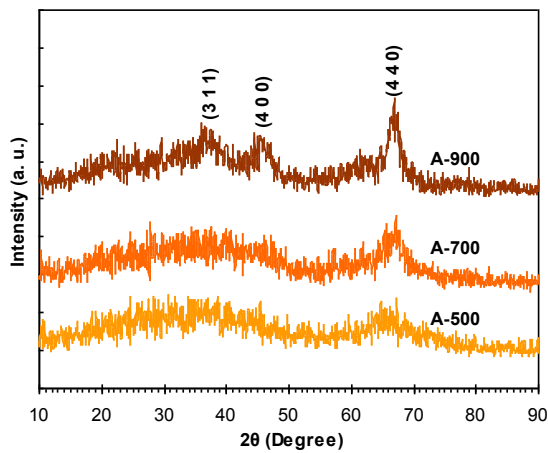


Fig. 2- X-ray diffraction patterns of pure  $\gamma$ -alumina (A) powders calcined at various temperatures.

revealed that there is no more crystallized phase at 500 °C. According to the related crystallographic habit plane (440), crystallization of gamma alumina phase from amorphous precursor occurred at about 700 °C while, there are no sign of the other transition phases. During further increment of the calcinations temperature to 900 °C, the other characteristic peak of the gamma alumina such as (400) and (311) have been emerged. The diffracted peaks are widened due to the deviation from the Bragg's law. This is a characteristic behavior for diffraction patterns of the nano-crystalline materials. Furthermore, crystallization of the other hydrated or transition alumina phases not observed.

The X-ray diffraction results of the sample AC, calcined at various temperatures, are shown in Fig. 3. The result for the sample AC-500, calcined at 500 °C, is similar to the sample A. there are no significant peaks of the  $\gamma$ -alumina at this temperature. While for the sample AC-700 the increment of the temperature cause to a noticeable sharpening in the peak intensity for (440) and (400) planes in comparison with the sample A-700 at figure 2. It obviously indicates the improvement of the crystallization of gamma alumina phase at this temperature at the presence of cationic addition of cobalt ions. During increment of the temperature to 900 °C the precursor well crystallized to gamma alumina and the other peaks have risen according to the JCPDS card 50-0741 [25]. The peak widening of the synthesized powders AC decreased at the presence of Co in comparison with the samples A. decreasing of the FWHM of the samples AC can be attributed to the cobalt effect in the facilitating and

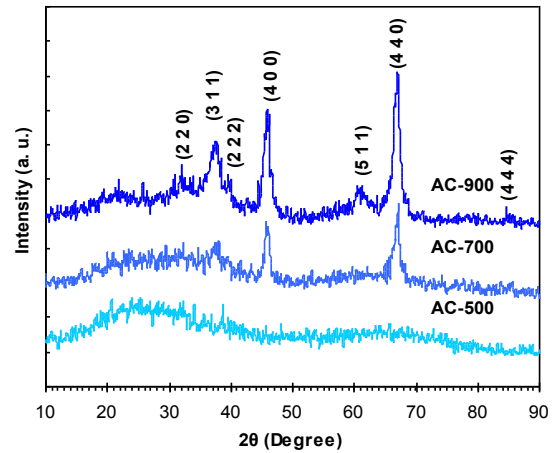


Fig. 3- X-ray diffraction patterns of  $\gamma$ -alumina + 1%mol.Co (AC) powders calcined at various temperatures.

lowering the temperature of crystallization. Also, it caused to increasing the degree of crystallinity and the size of the final particles.

Fig. 4 shows the nitrogen adsorption/desorption isotherms of samples A and AC calcined at 700 °C. In the International Union of Pure and Applied Chemistry (IUPAC) classification, there are three types of porous materials [8]. With respect to the pore diameters ( $r_p$ ) they are: micro-porous ( $r_p < 2$  nm), meso-porous ( $2 \text{ nm} < r_p < 50\text{nm}$ ) and macro-porous ( $50 \text{ nm} < r_p$ ). Both of A and AC hyseresis loops are related to the form H1 of the type IV. Theses materials have been classified as the mesoporous powders and include vertically parallel lines in the adsorption/desorption curves [26]. The two branches of the hysteresis loops are almost vertical and nearly parallel, which is consistent with H1 hysteresis loops of the  $N_2$  adsorption isotherms [15]. The loop of the AC sample moved to the high pressures value in comparison with the sample A. It shows the increasing of the pore size in AC samples

during grain growth occurring at the presence of Co addition.

Pore size distribution of A and AC samples that were calcined at 700 °C have been presented in Fig. 5. The size of the pores is below 10 nm that is the characteristic of the meso-porous materials. The distribution obtained by Barrett–Joyner–Halenda (BJH) technique from nitrogen adsorption/desorption isotherms. For sample AC the pore size shifted to higher value in both of the adsorption and desorption branches due to grain coarsening of the synthesized particles at the presence of the Co cations. Numerical result of BET and calculated size of the particles are listed in table 1. Particle size values were determined correspondent to BET method ( $G_{BET}$ ) using equation 1 and Scherrer method ( $G_{XRD}$ ) using FWHMs values. The value of gamma density was assumed 3.7 g/cm<sup>3</sup> in equation 1, as respect to the JCPDS card 50-0741. Specific surface area of the Co added sample is lower than the pure sample due to well crystallization and

Table 1- Specific surface area and particle size variation with gelatin amount

Sample	Specific surface area (m <sup>2</sup> /g)	G <sub>BET</sub> (nm)	mean pore size ( $r_p$ ) (nm)	G <sub>XRD</sub> (nm)
AC-700	140	11.6	5.5	11
A-700	186	8.7	6.5	7

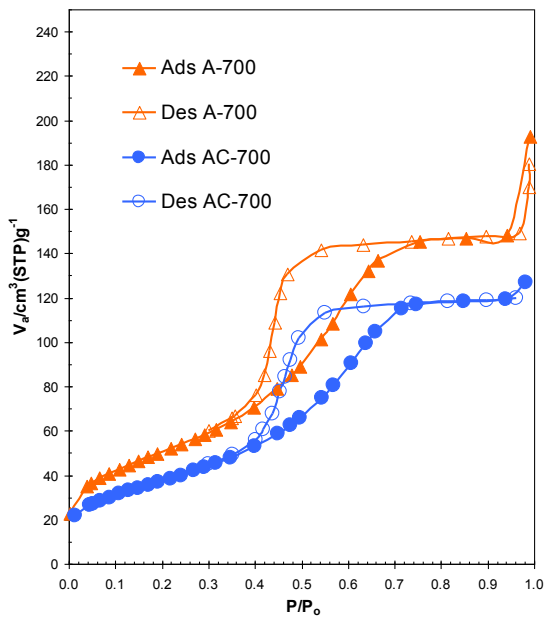


Fig. 4- Adsorption/desorption isotherms of A-700 and Ac-700 powders calcined at 700 °C.

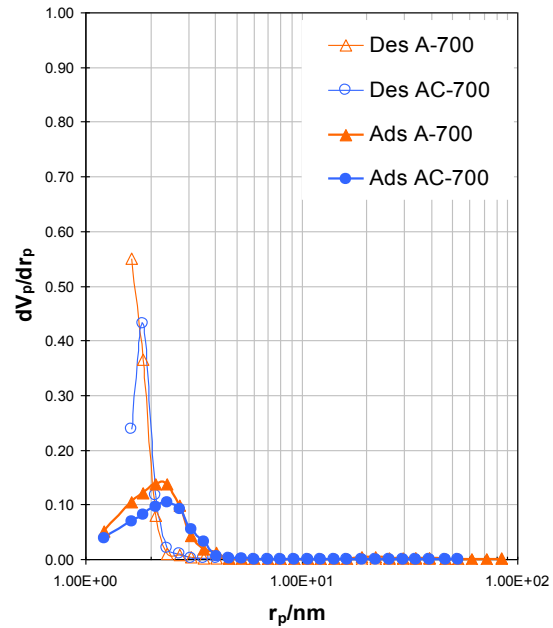


Fig. 5- Pore size distribution of A-700 and Ac-700 powders calcined at 700 °C.

grain coarsening at the calcination temperature 700 °C. Crystallite size of the particles,  $G_{XRD}$ , is nearly the same obtained value from SSA and it revealed that the most of the powders particles are single crystals. In addition, few decreasing in the mean pore size ( $r_p$ ) of AC-700 in comparison with the A-700 can be attributed to the partial sintering of the nano particles during calcination.

In agreement with the XRD and BET results

coarsening of the powders are shown in SEM micrograph at Fig. 6. The powders A-700 include a narrow distribution and AC-700 shows some aggregate particles during partial sintering that it lead to decreasing of the specific surface area and increasing the size of the grains.

Figure 7 shows the TEM and selected area electron diffraction (SAED) results for the A-700 and AC-700 samples. Related planes of diffracted

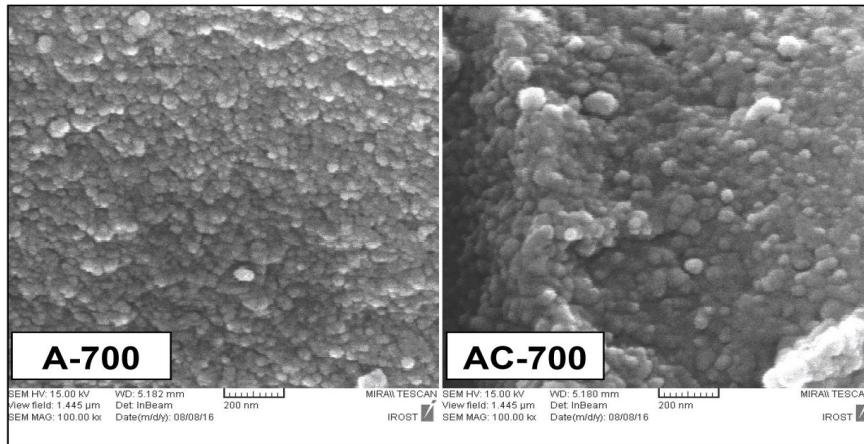


Fig. 6- FESEM micrograph of the A and AC powders calcined at 700 °C.

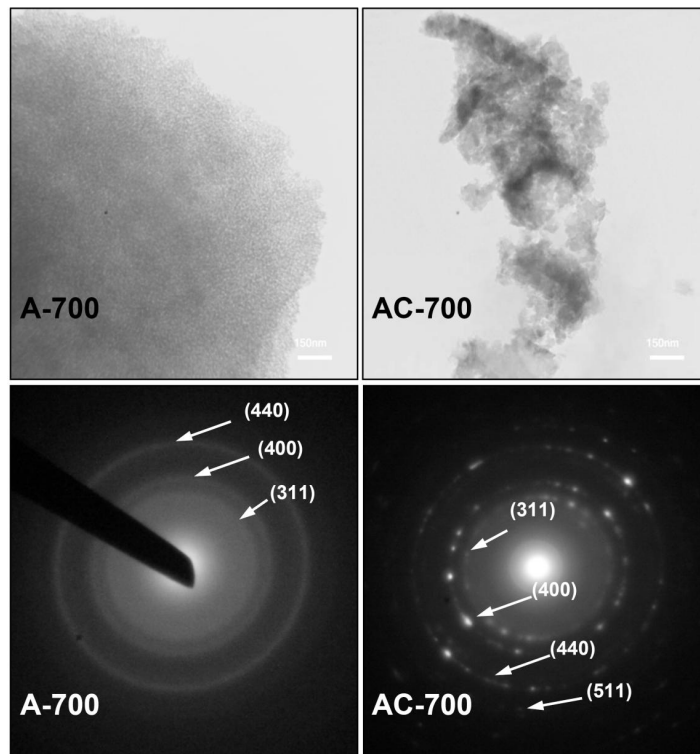


Fig. 7- TEM micrograph with SAED images of the A and AC powders calcined at 700 °C.

points of the gamma structure were solved by  $R_d = n\lambda$  formula [27]. TEM image of the sample A-700 indicate to the fine grains, while for AC-700 the particles are coarsened and aggregated. SAED of the A-700 contains the ring shape diffracted from the (311), (400) and (440) planes that is the characteristic of the fine and nano powders [18]. It contain some bright point of diffraction for AC-700 similar the crystalline materials.

#### 4- Conclusion

Cobalt addition in the aluminum nitrate solution causes the lowering synthesis temperature of the  $\gamma$ -alumina phase. Phase crystallization at the presence of 1 %mol cobalt cations occurs at about 200 °C lower than the pure precursor. Both hysteresis loops of the powders were in the form H1 of the type IV that classified meso-porous powders. Crystallite and grain size of the cobalt doped sample was coarser than the pure sample and specific surface area decreased from 186 to 140 m<sup>2</sup>/g in the presence of cobalt additive. Also, Cobalt doped powders show some bright point in the diffraction patterns of TEM due to its well crystallization in comparison with the pure powder.

#### References

1. Ksapabutr B, Gulari E, Wongkasemjit S. Sol-gel transition study and pyrolysis of alumina-based gels prepared from alumatrane precursor. *Colloids and Surfaces A: Physicochemical and Engineering Aspects*. 2004;233(1-3):145-53.
2. Trueba M, Trasatti SP.  $\gamma$ -Alumina as a Support for Catalysts: A Review of Fundamental Aspects. *European Journal of Inorganic Chemistry*. 2005;2005(17):3393-403.
3. Santos PS, Santos HS, Toledo SP. Standard transition aluminas. Electron microscopy studies. *Materials Research*. 2000;3(4):104-14.
4. Jiansirisomboon S, MacKenzie KJD. Sol-gel processing and phase characterization of Al<sub>2</sub>O<sub>3</sub> and Al<sub>2</sub>O<sub>3</sub>/SiC nanocomposite powders. *Materials Research Bulletin*. 2006;41(4):791-803.
5. Silva RA, Diniz CF, Viana MM, Abreu SL, Souza TGFd, Mohallem NDS, et al. Preparation of thin films using freeze drier alumina. *Brazilian Journal of Physics*. 2009;39(1a).
6. Aghayan M, Voltsihhin N, Rodríguez MA, Rubio-Marcos F, Dong M, Hussainova I. Functionalization of gamma-alumina nanofibers by alpha-alumina via solution combustion synthesis. *Ceramics International*. 2014;40(8):12603-7.
7. Samain L, Jaworski A, Edén M, Ladd DM, Seo D-K, Javier Garcia-Garcia F, et al. Structural analysis of highly porous  $\gamma$ -Al<sub>2</sub>O<sub>3</sub>. *Journal of Solid State Chemistry*. 2014;217:1-8.
8. Dabbagh HA, Shahraki M. Mesoporous nano rod-like  $\gamma$ -alumina synthesis using phenol-formaldehyde resin as a template. *Microporous and Mesoporous Materials*. 2013;175:8-15.
9. Nakano K, Ali SA, Kim H-J, Kim T, Alhooshani K, Park J-I, et al. Deep desulfurization of gas oil over NiMoS catalysts supported on alumina coated USY-zeolite. *Fuel Processing Technology*. 2013;116:44-51.
10. Díaz de León JN, Petranovskii V, de los Reyes JA, Alonso-Núñez G, Zepeda TA, Fuentes S, et al. One dimensional (1D)  $\gamma$ -alumina nanorod linked networks: Synthesis, characterization and application. *Applied Catalysis A: General*. 2014;472:1-10.
11. Chamack M, Mahjoub AR, Aghayan H. Catalytic performance of vanadium-substituted molybdophosphoric acid supported on zirconium modified mesoporous silica in oxidative desulfurization. *Chemical Engineering Research and Design*. 2015;94:565-72.
12. Wan Abdullah WN, Wan Abu Bakar WA, Ali R. Alumina supported polymolybdate catalysts utilizing tert-butyl hydroperoxide oxidant for desulfurization of Malaysian diesel fuel. *Korean Journal of Chemical Engineering*. 2015;32(10):1999-2006.
13. Gatan R, Barger P, Gembicki V. Oxidative desulfurization: A new technology for ULSD. American Chemical Society Division of Fuel Chemistry. 2004;49(2):577-579.
14. Abdullah WNW, Bakar WAWA, Ali R. Catalytic oxidative desulfurization of diesel fuel utilizing a polymolybdate alumina supported catalyst: characterization, catalytic activity and mechanistic study. *Reaction Kinetics, Mechanisms and Catalysis*. 2014;114(2):547-60.
15. Maldonado C, De la Rosa J, Lucio-Ortiz C, Hernández-Ramírez A, Barraza F, Valente J. Low Concentration Fe-Doped Alumina Catalysts Using Sol-Gel and Impregnation Methods: The Synthesis, Characterization and Catalytic Performance during the Combustion of Trichloroethylene. *Materials*. 2014;7(3):2062-86.
16. Pathak LC, Singh TB, Das S, Verma AK, Ramachandrarao P. Effect of pH on the combustion synthesis of nano-crystalline alumina powder. *Materials Letters*. 2002;57(2):380-5.
17. Shang X, Wang X, Nie W, Guo X, Zou X, Ding W, et al. Facile strategy for synthesis of mesoporous crystalline  $\gamma$ -alumina by partially hydrolyzing aluminum nitrate solution. *Journal of Materials Chemistry*. 2012;22(45):23806.
18. Zhou S, Antonietti M, Niederberger M. Low-Temperature Synthesis of  $\gamma$ -Alumina Nanocrystals from Aluminum Acetylacetonate in Nonaqueous Media. *Small*. 2007;3(5):763-7.
19. Badoga S, Sharma RV, Dalai AK, Adjaye J. Synthesis and characterization of mesoporous aluminas with different pore sizes: Application in NiMo supported catalyst for hydrotreating of heavy gas oil. *Applied Catalysis A: General*. 2015;489:86-97.
20. Ji X, Tang S, Gu L, Liu T, Zhang X. Synthesis of rod-like mesoporous  $\gamma$ -Al<sub>2</sub>O<sub>3</sub> by an ionic liquid-assisted sol-gel method. *Materials Letters*. 2015;151:20-3.
21. Sherikar BN, Umarji AM. Synthesis of  $\gamma$ -alumina by solution combustion method using mixed fuel approach (urea+ glycine fuel). *Int. J. Res. Eng. Technol*. 2013;5.
22. Ghosh S, Naskar MK. Synthesis of mesoporous  $\gamma$ -alumina nanorods using a double surfactant system by reverse microemulsion process. *RSC Advances*. 2013;3(13):4207.
23. Parida KM, Pradhan AC, Das J, Sahu N. Synthesis and characterization of nano-sized porous gamma-alumina by control precipitation method. *Materials Chemistry and Physics*. 2009;113(1):244-8.
24. Zhou M, Wei Z, Qiao H, Zhu L, Yang H, Xia T. Particle Size and Pore Structure Characterization of Silver Nanoparticles Prepared by Confined Arc Plasma. *Journal of Nanomaterials*. 2009;2009:1-5.
25. ASTM File 50-0741. Database PDF (Powder Diffraction File).
26. Sobhani M, Sedaghat A, Ebadzadeh T, Ebrahimi M. Preparation of nano-sized Mg 0.6 Al 0.8 Ti 1.6 O 5 powders using the inorganic salts route. *Ceramics International*. 2013;39(6):6899-905.
27. Attar A, Halali M, Sobhani M, Ghandehari RT. Synthesis of titanium nano-particles via chemical vapor condensation processing. *Journal of Alloys and Compounds*. 2011;509(19):5825-8.